A Comparison of OFDM-based Modulation Schemes for OWC with Clipping Distortion

A Comparison of OFDM-based Modulation Schemes for OWC with Clipping Distortion

Svilen Dimitrov, Sinan Sinanovic and Harald Haas

Institute for Digital Communications, Joint Research Institute for Signal and Image Processing, The University of Edinburgh, EH9 3JL Edinburgh, UK, e-mail: {s.dimitrov, s.sinanovic, h.haas}@ed.ac.uk

***Abstract*—In this paper, the electrical power requirement and spectral efficiency of multi-carrier transmission schemes for optical wireless communications (OWC) are compared in the presence of front-end-induced double-sided signal clipping. The two existing multi-carrier modulation techniques based on orthogonal frequency division multiplexing (OFDM), direct-current-biased optical OFDM (DCO-OFDM) and asymmetrically clipped optical OFDM (ACO-OFDM), are studied. The clipping noise can be modeled according to the Bussgang theorem and the central limit theorem (CLT) as attenuation of the data-carrying subcarriers and addition of zero-mean complex-valued Gaussian noise. Presented closed-form expressions for the attenuation factor and the clipping noise variance are employed in the derivation of the electrical signal-to-noise ratio (SNR). Paired with multi-level quadrature amplitude modulation (M-QAM), the electrical power requirement of optical OFDM (O-OFDM) transmission is obtained from the bit-error ratio (BER) system performance. It is shown that in a practical front-end biasing setup DCO-OFDM has a lower electrical power requirement to achieve a target BER as compared to ACO-OFDM for modulation orders with equal spectral efficiencies above 1 bit/s/Hz.**

***Index Terms*—DCO-OFDM, ACO-OFDM, optical wireless communication, clipping noise, emitter biasing, detector noise.**

I. Introduction

OWC is a promising candidate for medium range high-speed data transmission. Both infrared [1] and visible light communication [2] have the potential to deliver several hundreds of Mbps throughput. In addition to being a complementary non-interfering solution alongside radio frequency (RF) technology, OWC has the advantage of license-free operation over a significantly wider spectrum.

The data transmission in OWC is achieved through intensity modulation and direct detection (IM/DD). A real-valued non-negative signal modulates the intensity of a light emitting diode (LED) at the transmitter, and it is detected by a photo-diode (PD) at the receiver. Multi-carrier modulation such as M-QAM O-OFDM has inherent robustness to the multi-path dispersion of the optical wireless channel, and it promises to deliver very high data rates [2]. In the literature, two possible O-OFDM system realizations can be found: DCO-OFDM [3] and ACO-OFDM [4]. A real-valued signal is obtained, when Hermitian symmetry is imposed on the OFDM subcarriers. A non-negative signal is obtained in DCO-OFDM by the addition of a direct current (DC) bias. In ACO-OFDM, the odd subcarriers are enabled for data transmission, whereas the even ones are set to zero. Here, the negative part of the time domain signal can be clipped at the transmitter, and the information can be still successfully decoded from the odd subcarriers at the receiver. As a result, ACO-OFDM presents a greater optical power efficiency at the expense of a 50% reduction in spectral efficiency as compared to DCO-OFDM. The two systems have been compared in terms of optical power requirement and spectral efficiency in [5] in an idealized front-end biasing setup, where a non-negative signal can turn on the LED, and the transmitter has an infinite dynamic range. Such conditions, however, are hardly achievable in practice. In addition, a comparison in terms of electrical power requirement, including both alternating current (AC) power and DC power, and spectral efficiency in a practical front-end biasing setup is considered an open issue.

The imperfections of the optical front-ends due to the use of off-the-shelf components result in a limited linear dynamic range of radiated optical power. In general, the transmitter LED is biased by a constant current source, which supports the entire range of forward voltages across the LED. The bias current is added to the information carrying current, yielding the forward current through the LED. Since the radiated optical power is directly proportional to the forward current, the signal and the transmitter constraints are described in terms of optical power in the rest of the paper. It is shown in [6] that the non-linear I-V characteristic of the LED can be compensated by pre-distortion. A linear characteristic is obtainable, however, only over a limited range between $i_{\min}$ and $i_{\max}$, corresponding to a point of minimum optical power, $P_{\mathrm{Tx,min}}$, and a point of maximum optical power, $P_{\mathrm{Tx,max}}$. Furthermore, the eye safety regulations [7] and/or the design requirements constrain the level of radiated average optical power to $P_{\mathrm{Tx,avg}}$. In order to condition the signal in accord with these constraints, signal scaling in the digital signal processor (DSP) and DC-biasing in the analog circuitry is required. Because of the fact that an OFDM system employs the unitary inverse fast Fourier transform (IFFT) as a multiplexing technique at the transmitter, the non-clipped signal follows a close to Gaussian distribution for IFFT sizes greater than 64 [8], according to the CLT. Therefore, signal shaping in DCO-OFDM and ACO-OFDM, in order to fit the front-end power constraints, results in a non-linear signal distortion. Using the fact that the unitary fast Fourier transform (FFT) is employed as a demultiplexing technique at the receiver, the non-linear distortion can be modeled by means of the Bussgang theorem and CLT as attenuation of the information carrying subcarriers plus zero-

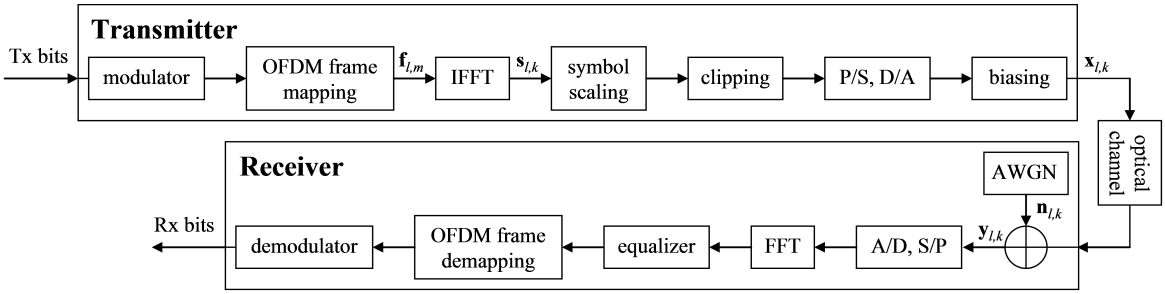

Fig. 1: Block diagram of O-OFDM transmission.

mean complex-valued Gaussian noise [9]. In the previous study, closed-form expressions for the attenuation factor and the clipping noise variance are determined for ACO-OFDM as a function of the independent bottom and top clipping levels. Symmetric signal clipping in DCO-OFDM has been analyzed in [10], whereas the signal clipping at independent bottom and top levels is still considered an open issue.

In this paper, double-sided signal clipping at the transmitter front-end is studied for DCO-OFDM and ACO-OFDM. The attenuation factor and the variance of the complex-valued Gaussian clipping noise at the received data-carrying subcarriers are determined in closed-form and included in the derivation of the effective electrical SNR. The O-OFDM systems are compared in a novel fashion in terms of electrical power requirement and spectral efficiency in a practical front-end biasing setup with several double-sided signal clipping scenarios. DCO-OFDM demonstrates a lower electrical power requirement to achieve a target BER for QAM modulation orders with spectral efficiencies above 1 bit/s/Hz. Equivalently, DCO-OFDM delivers higher throughput as compared to ACO-OFDM for SNR targets above 16 dB.

The rest of the paper is organized as follows. Section II presents the O-OFDM system model. DCO-OFDM and ACO-OFDM are compared in terms of electrical power requirement and spectral efficiency in Section III. Finally, Section IV concludes the paper.

II. O-OFDM TRANSMISSION

The conventional discrete model for a noisy communication link is employed in this study:

$$\mathbf{y} = \mathbf{h} * \mathbf{x} + \mathbf{n}\,, \tag{1}$$

where $\mathbf{y}$ represents the received distorted replica of the transmitted signal $\mathbf{x}$, which is convolved with the channel impulse response, $\mathbf{h}$, and additive white Gaussian noise (AWGN), $\mathbf{n}$, is added at the receiver. In M-QAM O-OFDM, $\mathbf{n}$ represents a bipolar real-valued zero-mean Gaussian noise, which after optical-to-electrical (O/E) conversion is transformed into a complex-valued AWGN with an electrical power spectral density (PSD) of $N_0/2$ per complex dimension [11]. Here, $*$ stands for discrete linear convolution. The discrete signal vectors are obtained after sampling of the equivalent continuous-time signals with a sampling period of T. Here, $\mathbf{x}$ contains $Z_{\mathbf{x}}$ samples, $\mathbf{h}$ has $Z_{\mathbf{h}}$ samples, and as a result, $\mathbf{n}$ and $\mathbf{y}$ have $Z_{\mathbf{x}} + Z_{\mathbf{h}} - 1$ samples [11]. In multi-carrier systems, the optical wireless channel is transformed into a flat fading channel with an optical path gain, $g_{\mathrm{h(opt)}}$ [12], by the use of a large number of subcarriers and a cyclic prefix (CP). The CP transforms the linear convolution into a cyclic convolution. Therefore, single-tap zero forcing (ZF) or minimum mean-squared error (MMSE) equalization is sufficient to counter the channel effect. Since the CP has a negligible effect on the electrical power requirement or the spectral efficiency [13], it is omitted in the derivations in this study. The signal shaping framework for $\mathbf{x}$ is elaborated below.

The block diagram for multi-carrier O-OFDM transmission is presented in Fig. 1. Here, $\log_2(M)$ bits of the equiprobable input bits modulate the complex-valued information carrying frequency domain subcarrier in an M-QAM fashion. In general, N subcarriers form the l-th OFDM frame, $\mathbf{f}_{l,m}$, $l = 0, 1, ..., L-1$, corresponding to the l-th OFDM symbol, where m, $m = 0, 1, ..., N-1$, is the subcarrier index. Each subcarrier occupies a bandwidth of $1/NT$ in a total OFDM frame bandwidth of $1/T$. Both systems have the Hermitian symmetry imposed on the OFDM frame, in order to ensure a real-valued time domain signal. Whereas in DCO-OFDM the information carrying subcarriers populate the first half of the frame, leaving the first one set to zero, in ACO-OFDM every even subcarrier is set to zero. The l-th OFDM symbol in the train of L symbols, $\mathbf{s}_l$, is obtained by the IFFT of the l-th OFDM frame in the train of L frames, $\mathbf{f}_l$. Here, the time domain sample index within the l-th OFDM symbol, $\mathbf{s}_{l,k}$, is denoted by k, $k = 0, 1, ..., N-1$. As a result, the time domain OFDM symbol with a bandwidth of $1/T$ has a duration of NT [11]. The resulting spectral efficiency of DCO-OFDM is $\log_2(M)(N-2)/(2N)$ bits/s/Hz, whereas ACO-OFDM achieves $\log_2(M)/4$ bits/s/Hz. The train of OFDM symbols, $\mathbf{s}_{l,k}$, follows a close to Gaussian distribution for IFFT/FFT sizes greater than 64 [8]. In order to fit the signal within the limited linear dynamic range of the transmitter, $\mathbf{s}_{l,k}$ is scaled and clipped at normalized bottom and top clipping levels of $\lambda_{\mathrm{bottom}}$ and λ_{top} relative to a standard normal distribution [9]. In addition, because of the structure of the ACO-OFDM frame, the negative samples of the ACO-OFDM time domain signal can be clipped, and the information can still be successfully decoded from the odd subcarriers at the receiver. Next, the train of symbols is subjected to a parallel-to-

serial (P/S) conversion, and it is passed through the digital-to-analog (D/A) converter. Here, a pulse shaping filter is applied to obtain a continuous-time signal. In the analog circuitry the signal is DC-biased by β_{DC}. Therefore, the transmitted signal vector, $\mathbf{x}$, with a length of $Z_{\mathbf{x}} = LN$ can be expressed as follows:

$$\mathbf{x}_{l,k} = \mathrm{CLIP}\left[\alpha_l \mathbf{s}_{l,k}\right] + \beta_{\mathrm{DC}} \; . \tag{2}$$

Here, α_l is given for a particular OFDM symbol as follows [9]:

$$\alpha_l = \sigma \sqrt{\frac{N-1}{\sum_{m=0}^{N-1} |\mathbf{f}_{l,m}|^2}} \; , \tag{3}$$

where σ is the target standard deviation of the non-clipped time domain signal to be fit within the front-end optical power constraints. Note that $\mathrm{E}\left[\alpha_l^2\right]$ can be simplified to $\mathrm{E}\left[\alpha_l^2\right] = b\sigma^2$. Here, b is the inverse bandwidth utilization factor, *i.e.* $b = (N-2)/N$ in DCO-OFDM and $b = 2$ in ACO-OFDM. Therefore, the information carrying subcarriers have an average electrical symbol power of $E_{\mathrm{s(elec)}} = E_{\mathrm{b(elec)}} \log_2(M) = b\sigma^2$, where $E_{\mathrm{b(elec)}}$ is the average electrical bit power. The non-linear clipping distortion represented by the $\mathrm{CLIP}\left[\cdot\right]$ operator can be translated into an attenuation factor, K, on the information carrying subcarriers plus a zero-mean complex-valued Gaussian noise component with a variance of σ^2_{clip} [9]. In DCO-OFDM and ACO-OFDM, K is given as follows [9]:

$$K = Q(\lambda_{\mathrm{bottom}}) - Q(\lambda_{\mathrm{top}}) \; . \tag{4}$$

Here, $Q(\cdot)$ stands for the complementary cumulative distribution function (CCDF) of a standard normal distribution with zero mean and unity variance. The variance of the clipping noise can be expressed in ACO-OFDM as follows [9]:

$$\begin{aligned} \sigma^2_{\mathrm{clip}} = \frac{E_{\mathrm{s(elec)}}}{2}\Big(& K\left(\lambda^2_{\mathrm{bottom}} + 1\right) - 2K^2 \\ & - \lambda_{\mathrm{bottom}}\left(\phi(\lambda_{\mathrm{bottom}}) - \phi(\lambda_{\mathrm{top}})\right) \\ & - \phi(\lambda_{\mathrm{top}})\left(\lambda_{\mathrm{top}} - \lambda_{\mathrm{bottom}}\right) \\ & + Q(\lambda_{\mathrm{top}})\left(\lambda_{\mathrm{top}} - \lambda_{\mathrm{bottom}}\right)^2\Big) \; , \end{aligned} \tag{5}$$

where $\phi(\cdot)$ stands for the probability density function (PDF) of a standard normal distribution. Following the procedure elaborated in [9], the variance of the clipping noise in DCO-OFDM can be expressed as follows:

$$\begin{aligned} \sigma^2_{\mathrm{clip}} = E_{\mathrm{s(elec)}}\Big(& K - K^2 - \left(\phi(\lambda_{\mathrm{bottom}}) - \phi(\lambda_{\mathrm{top}})\right. \\ & \left. + (1 - Q(\lambda_{\mathrm{bottom}}))\lambda_{\mathrm{bottom}} + Q(\lambda_{\mathrm{top}})\lambda_{\mathrm{top}}\right)^2 \\ & + (1 - Q(\lambda_{\mathrm{bottom}}))\lambda^2_{\mathrm{bottom}} + Q(\lambda_{\mathrm{top}})\lambda^2_{\mathrm{top}} \\ & + \phi(\lambda_{\mathrm{bottom}})\lambda_{\mathrm{bottom}} - \phi(\lambda_{\mathrm{top}})\lambda_{\mathrm{top}}\Big) \; . \end{aligned} \tag{6}$$

The attenuation factor, K, as a function of the clipping levels is presented in Fig. 2 and Fig. 3 in DCO-OFDM and ACO-OFDM. The respective clipping noise variance, σ^2_{clip}, is illustrated in Fig. 4 and Fig. 5. Here, a large symbol distortion is defined for a small K and large σ^2_{clip}. Therefore, Fig. 2 and Fig. 4 suggest that the symbol distortion in DCO-OFDM can be minimized with symmetric clipping levels. In addition, Fig. 3 and Fig. 5 show that downside clipping introduces a larger ACO-OFDM symbol distortion than upside clipping.

In addition to the distortion of the information carrying subcarriers, time domain signal clipping modifies the average optical power of the transmitted signal as follows:

$$\begin{aligned} \mathrm{E}\left[\mathbf{x}\right] = \sigma\Big(& \lambda_{\mathrm{top}} Q(\lambda_{\mathrm{top}}) - \lambda_{\mathrm{bottom}} Q(\lambda_{\mathrm{bottom}}) \\ & + \phi(\lambda_{\mathrm{bottom}}) - \phi(\lambda_{\mathrm{top}})\Big) + P_{\mathrm{bottom}} \; . \end{aligned} \tag{7}$$

In DCO-OFDM, $P_{\mathrm{bottom}} = P_{\mathrm{Tx,min}}$. In ACO-OFDM, $P_{\mathrm{bottom}} = \max\Big(P_{\mathrm{Tx,min}}, \beta_{\mathrm{DC}}\Big)$ because of the default zero-level clipping. In general, the eye safety regulations [7] and/or the design requirements impose the constraint: $\mathrm{E}\left[\mathbf{x}\right] \leq P_{\mathrm{Tx,avg}}$. Since the signal is clipped, the resulting average optical signal power, $\mathrm{E}\left[\mathbf{x}\right]$, is not equal to the average optical symbol power, $E_{\mathrm{s(opt)}}$. In general, $E_{\mathrm{s(opt)}}$, is defined for the scenario with the least signal clipping, which is given in DCO-

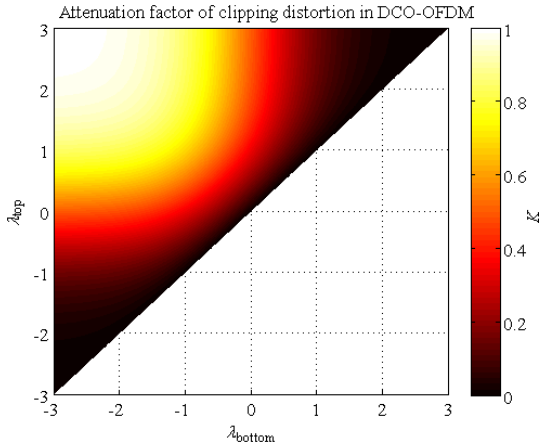

Fig. 2: Attenuation factor, K, in DCO-OFDM as a function of the normalized clipping levels.

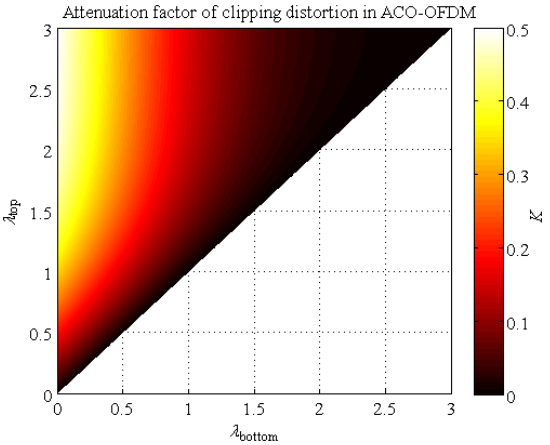

Fig. 3: Attenuation factor, K, in ACO-OFDM as a function of the normalized clipping levels.

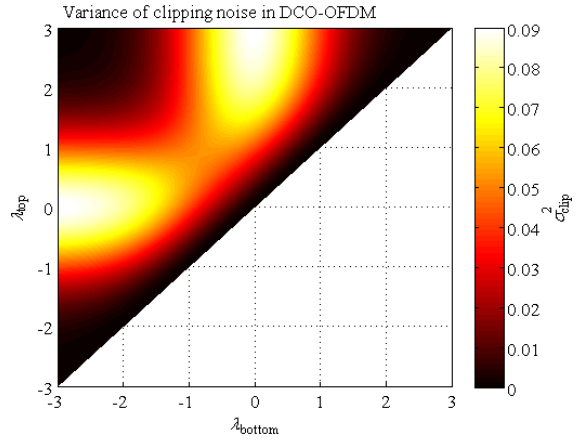

Fig. 4: Clipping noise variance, σ^2_{clip}, in DCO-OFDM as a function of the normalized clipping levels. Here, $E_{\text{s(elec)}} = 1$.

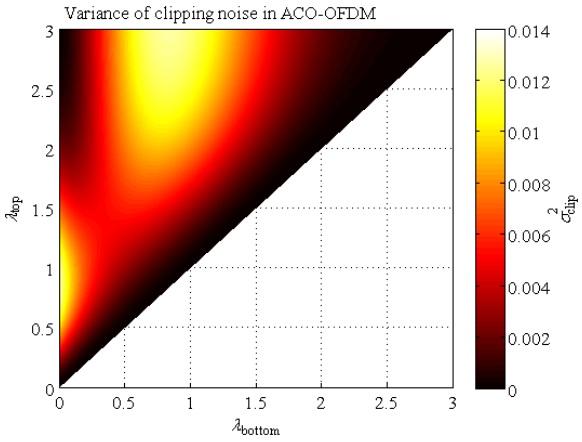

Fig. 5: Clipping noise variance, σ^2_{clip}, in ACO-OFDM as a function of the normalized clipping levels. Here, $E_{\text{s(elec)}} = 1$.

OFDM as $\lambda_{\text{bottom}} = -\infty$ and $\lambda_{\text{top}} = +\infty$, and in ACO-OFDM as $\lambda_{\text{bottom}} = 0$ and $\lambda_{\text{top}} = +\infty$. Thus, in DCO-OFDM, $E_{\text{s(opt)}} = \beta_{\text{DC}}$, whereas in ACO-OFDM, $E_{\text{s(opt)}} = (\beta_{\text{DC}} + \sigma/\sqrt{2\pi})$. Combined with (7), these equations convey the relation between $\mathrm{E}[\mathbf{x}]$ and $E_{\text{s(opt)}}$.

The E/O conversion given in [5] can be generalized in DCO-OFDM and ACO-OFDM, respectively, as follows:

$$E_{\text{s(opt)}} = \sqrt{\frac{\mathrm{E}[\mathbf{x}]^2}{\mathrm{E}[\mathbf{x}^2]} E_{\text{s(elec)}}} = \sqrt{\frac{\beta^2_{\text{DC}}}{\sigma^2 + \beta^2_{\text{DC}}} E_{\text{s(elec)}}}\,, \tag{8}$$

$$E_{\text{s(opt)}} = \sqrt{\frac{2\pi\beta^2_{\text{DC}} + 2\sigma\beta_{\text{DC}}\sqrt{2\pi} + \sigma^2}{2\pi\beta^2_{\text{DC}} + 2\sigma\beta_{\text{DC}}\sqrt{2\pi} + \pi\sigma^2} E_{\text{s(elec)}}}\,. \tag{9}$$

Here, $\mathrm{E}[\mathbf{x}]$ and $\mathrm{E}[\mathbf{x}^2]$ are defined for the least signal clipping scenario, and these are used in every other clipping setup.

The signal $\mathbf{x}_{l,k}$ is transmitted over the optical wireless channel, and it picks up AWGN, $\mathbf{n}_{l,k}$, at the receiver to obtain $\mathbf{y}_{l,k}$. In the analog-to-digital (A/D) converter, the signal is passed through a matched filter, and it is sampled at a frequency of $1/T$ [11]. Using a serial-to-parallel (S/P) converter, the signal is passed through an FFT block back to the frequency domain. After ZF or MMSE equalization, a hard-decision decoder is employed on the known OFDM frame structure to obtain the received bits. Thus, the effective electrical SNR per bit in O-OFDM is given as follows [9]:

$$\Gamma_{\text{b(elec)}} = \frac{K^2 E_{\text{b(elec)}}}{\sigma^2_{\text{clip}} + \dfrac{N_0}{bG_{\text{EQ}}G_{\text{DC}}}}\,, \tag{10}$$

where G_{EQ} stands for the equalizer gain, and it is given for ZF and MMSE, respectively, as $g^2_{\text{h(opt)}}$ and $g^2_{\text{h(opt)}} + \left(E_{\text{b(elec)}}/N_0\right)^{-1}$. Here, G_{DC} denotes the attenuation of the useful electrical signal power of $\mathbf{x}$ due to the DC component, and it can be expressed in DCO-OFDM and ACO-OFDM, respectively, as follows:

$$G_{\text{DC}} = \frac{\mathrm{E}\left[(\mathbf{x} - \beta_{\text{DC}})^2\right]}{\mathrm{E}[\mathbf{x}^2]} = \frac{\sigma^2}{\sigma^2 + \beta^2_{\text{DC}}}\,, \tag{11}$$

$$G_{\text{DC}} = \frac{\sqrt{2\pi}\sigma^2}{\sqrt{2\pi}\sigma^2 + 4\sigma\beta_{\text{DC}} + 2\sqrt{2\pi}\beta^2_{\text{DC}}}\,. \tag{12}$$

The factor G_{DC} is defined for the least signal clipping scenario, and it is used in every other clipping setup.

The BER performance of M-QAM O-OFDM in AWGN can be obtained as follows [14]:

$$\text{BER} = \frac{4\left(\sqrt{M}-1\right)}{\log_2(M)\sqrt{M}} Q\left(\sqrt{\frac{3\log_2(M)}{M-1}\Gamma_{\text{b(elec)}}}\right)\,. \tag{13}$$

III. Electrical power requirement *vs.* spectral efficiency in O-OFDM

DCO-OFDM and ACO-OFDM are compared in terms of electrical power requirement to achieve a target BER of 10^{-3} and the corresponding spectral efficiency. Here, the electrical power is normalized by the noise power for unity bandwidth, *i.e.* the electrical SNR per bit, $E_{\text{b(elec)}}/N_0$. The following modulation orders are chosen, $M = \{2, 4, 16, 64, 256, 1024\}$. Here, the case of $M = 2$ is realized in M-QAM through binary phase shift keying (BPSK) modulation, which requires the same $E_{\text{b(elec)}}/N_0$ as 4-QAM at the expense of 50% reduction in spectral efficiency. A practical linear dynamic range of a Vishay TSHG8200 LED between $P_{\text{Tx,min}} = 5$ mW and $P_{\text{Tx,max}} = 50$ mW at room temperature is considered at the transmitter [15]. Since this LED is eye-safe, even if operated at $P_{\text{Tx,max}} = 50$ mW [12], no constraint is imposed on the average optical power level. As suggested in Fig. 2 and Fig. 4, the non-linear clipping distortion in DCO-OFDM can be minimized, when symmetrical clipping levels are considered, *i.e.* $\lambda_{\text{bottom}} = -\lambda_{\text{top}}$. According to Fig. 3 and Fig. 5 the distortion in ACO-OFDM is minimum, when the bottom level clipping is kept at minimum, *i.e.* $\lambda_{\text{bottom}} = 0$. Therefore, the average optical power level in DCO-OFDM is set to $\mathrm{E}[\mathbf{x}] = \beta_{\text{DC}} = 27.5$ mW. In ACO-OFDM, $\mathrm{E}[\mathbf{x}]$ can be obtained from (7), where $\beta_{\text{DC}} = 5$ mW. The variance of the time domain signal, σ^2, results from the choice of the normalized top clipping level, λ_{top}. Here, $\lambda_{\text{top}} = \{2, 3, 4\}$ is

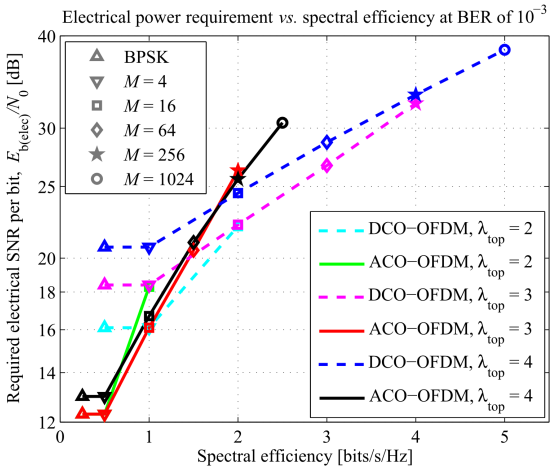

Fig. 6: Electrical power requirement *vs.* spectral efficiency at 10^{-3} BER of DCO-OFDM and ACO-OFDM.

considered, in order to illustrate the influence of the biasing setup on the electrical power requirement and the spectral efficiency of the O-OFDM systems. In addition, since the optical path gain coefficient, $g_{\mathrm{h(opt)}}$, directly translates into an SNR penalty in (10), $g_{\mathrm{h(opt)}} = 1$ is assumed for simplicity. An MMSE equalizer is used.

The power requirement *vs.* spectral efficiency plot of DCO-OFDM and ACO-OFDM is presented in Fig. 6. It is shown that ACO-OFDM requires an SNR of 12.3 dB, in order to enable BPSK and 4-QAM transmission. In order to enable BPSK and 4-QAM transmission in DCO-OFDM, an SNR of 16 dB is required. However, it is shown that for modulation orders with spectral efficiencies greater than 1 bit/s/Hz DCO-OFDM has a lower electrical power requirement as compared to ACO-OFDM to achieve the target BER of 10^{-3}. Equivalently, DCO-OFDM delivers higher throughput for SNR targets above 16 dB. In addition, it is shown that the electrical power requirement and the spectral efficiency of the O-OFDM systems greatly depend on the choice of the biasing setup. A lower λ_{top} value corresponds to a higher signal variance and a lower SNR target. However, such a scenario is unable to realize higher order modulation because of the increased nonlinear clipping distortion. A higher λ_{top} value corresponds to a lower signal variance, which requires a higher SNR target, but it enables higher order modulation, *e.g.* 1024-QAM.

IV. Conclusion

In this paper, double-sided signal clipping in DCO-OFDM and ACO-OFDM is studied. In accord with the Bussgang theorem and the CLT, the statistics of the clipping noise at the received data-carrying subcarriers are presented in closed-form as a function of the normalized bottom and top clipping levels. The derived expression for the effective electrical SNR in optical OFDM is employed to obtain the electrical power requirement to achieve a target BER of 10^{-3}. As a result, DCO-OFDM and ACO-OFDM are compared in a novel fashion in terms of electrical power requirement and spectral efficiency in a practical front-end biasing setup for several clipping scenarios. DCO-OFDM demonstrates a lower electrical power requirement for modulation orders with spectral efficiency above 1 bit/s/Hz. Equivalently, DCO-OFDM shows a greater spectral efficiency for SNR targets above 16 dB. While a higher signal variance reduces the SNR target, it introduces a larger clipping distortion, which prevents the realization of higher order QAM. Even though a lower signal variance increases the SNR target, it reduces the clipping distortion, which enables higher order QAM and the highest system throughput.

Acknowledgement

We gratefully acknowledge EADS UK Ltd. for the support of this research. Professor Haas acknowledges the Scottish Funding Council support of his position within the Edinburgh Research Partnership in Engineering and Mathematics between the University of Edinburgh and Heriot Watt University.

References

[1] F. R. Gfeller and U. Bapst, "Wireless In-House Data Communication Via Diffuse Infrared Radiation," *Proceedings of the IEEE*, vol. 67, no. 11, pp. 1474–1486, Nov. 1979.

[2] Y. Tanaka, T. Komine, S. Haruyama, and M. Nakagawa, "Indoor Visible Communication Utilizing Plural White LEDs as Lighting," in *Proceedings of the* 12^{th} *IEEE International Symposium on Personal, Indoor and Mobile Radio Communications*, vol. 2, San Diego, CA, USA, Sep. 30–Oct. 3, 2001, pp. 81–85.

[3] J. B. Carruthers and J. M. Kahn, "Multiple-subcarrier Modulation for Nondirected Wireless Infrared Communication," *IEEE Journal on Selected Areas in Communications*, vol. 14, no. 3, pp. 538–546, Apr. 1996.

[4] J. Armstrong and A. Lowery, "Power Efficient Optical OFDM," *Electronics Letters*, vol. 42, no. 6, pp. 370–372, Mar. 16, 2006.

[5] J. Armstrong and B. J. C. Schmidt, "Comparison of Asymmetrically Clipped Optical OFDM and DC-Biased Optical OFDM in AWGN," *IEEE Commun. Lett.*, vol. 12, no. 5, pp. 343–345, May 2008.

[6] H. Elgala, R. Mesleh, and H. Haas, "Non-linearity effects and predistortion in optical OFDM wireless transmission using LEDs," *Inderscience Intenational Journal of Ultra Wideband Communications and Systems (IJUWBCS)*, vol. 1, no. 2, pp. 143–150, 2009.

[7] BS EN 62471:2008, *Photobiological Safety of Lamps and Lamp Systems*, BSI British Standards Std., Sep. 2008.

[8] D. Dardari, V. Tralli, and A. Vaccari, "A Theoretical Characterization of Nonlinear Distortion Effects in OFDM Systems," *IEEE Transactions on Communications*, vol. 48, no. 10, pp. 1755–1764, Oct. 2000.

[9] S. Dimitrov, S. Sinanovic, and H. Haas, "Double-sided Signal Clipping in ACO-OFDM Wireless Communication Systems," in *IEEE International Conference on Communications (IEEE ICC 2011)*, Kyoto, Japan, 5–9 Jun. 2011.

[10] S. Randel, F. Breyer, S. C. J. Lee, and J. W. Walewski, "Advanced Modulation Schemes for Short-Range Optical Communications," *IEEE Journal of Selected Topics in Quantum Electronics*, vol. PP, no. 99, pp. 1 –10, 2010.

[11] D. Tse and P. Viswanath, *Fundamentals of Wireless Communication*. Cambridge University Press, 2005.

[12] S. Dimitrov, R. Mesleh, H. Haas, M. Cappitelli, M. Olbert, and E. Bassow, "On the SIR of a Cellular Infrared Optical Wireless System for an Aircraft," *IEEE Journal on Selected Areas in Communications (IEEE JSAC)*, vol. 27, no. 9, pp. 1623–1638, Dec. 2009.

[13] H. Elgala, R. Mesleh, and H. Haas, "Practical Considerations for Indoor Wireless Optical System Implementation using OFDM," in *Proc. of the IEEE 10th International Conference on Telecommunications (ConTel)*, Zagreb, Croatia, Jun. 8–10 2009.

[14] I. A. Glover and P. M. Grant, *Digital Communications*, 2nd ed. Pearson Prentice Hall, 2004.

[15] Vishay Semiconductors, "Datasheet: TSHG8200 High Speed Infrared Emitting Diode, 830 nm, GaAlAs Double Hetero," Retrieved Jul. 26, 2011 from http://www.vishay.com/docs/84755/tshg8200.pdf, Jul. 2008.